

## A Fourteen-Band Photometric Study of A2443 \*

Zhong-Lue Wen<sup>1</sup>, Yan-Bin Yang<sup>1</sup>, Qi-Rong Yuan<sup>2</sup>, Xu Zhou<sup>1</sup>, Jun Ma<sup>1</sup> and Zhao-Ji Jiang<sup>1</sup>

<sup>1</sup> National Astronomical Observatories, Chinese Academy of Sciences, Beijing 100012  
*zhonglue@bao.ac.cn*

<sup>2</sup> Department of Physics, Nanjing Normal University, Nanjing 210097

Received 2006 May 15; accepted 2006 December 2

**Abstract** We present a multi-color photometric study of the galaxy cluster A2443 ( $z = 0.108$ ) with the Beijing-Arizona-Taiwan-Connecticut (BATC) system. The spectral energy distributions (SEDs) in 14 intermediate bands are obtained for 5975 detected from  $\sim 1 \text{ deg}^2$  of the BATC images. Color-color diagrams are used for star-galaxy separation, then a photometric redshift technique is applied to the galaxy sample for cluster membership determination. There are 301 galaxies with photometric redshifts between 0.08 and 0.14 determined as member candidates of A2443, including 289 new ones. Based on this enlarged sample, the luminosity function and color magnitude relation of the cluster are studied. With an evolutionary synthesis model, we find that the fainter galaxies tend to have longer time scales of star formation than the brighter ones. Morphologically, we show an elongated spatial distribution associating with the galaxy cluster ZwCl 2224.2+1651, which contains more blue galaxies. This result indicates that galaxy cluster ZwCl 2224.2+1651 may be falling into A2443, and cluster-cluster interaction could have triggered star formation activities in ZwCl 2224.2+1651.

**Key words:** galaxies: clusters: individual: A2443 — galaxies: distances and redshifts

### 1 INTRODUCTION

As the largest gravitational bound systems in the universe, clusters of galaxies are important laboratories for understanding the evolution of galaxies, and for constraining cosmological quantities (Bahcall 1988; Postman et al. 1992; Brunner & Lubin 2000; Pearce et al. 2000; Cortese et al. 2004). The morphologies and dynamical states of galaxy clusters may shed light on the theories of large-scale structure formation (Kauffmann et al. 1999). For example, hierarchical clustering model predicts that galaxy clusters are formed by accreting nearby groups and galaxies along filaments (Zeldovich et al. 1982; West et al. 1991, 1995; Colberg et al. 2000). Studies have revealed that a high fraction of galaxy clusters shows substructures (Bird 1994; Mohr et al. 1993; Escalera et al. 1994), implying that these clusters depart from equilibrium and are still at the stage of merging. Such dynamics can be directly identified from the X-ray images (Nikogossyan et al. 1999), also inferred from the substructures shown in the optical band (Baier 1977; Dressler & Shectman 1988; Colless & Dunn 1996).

A2443 is a rich cluster ( $z = 0.108$ , Struble & Rood 1999) of richness 2 (Abell 1958) and Bautz-Morgan type II (McHardy 1974), centered at  $22^{\text{h}}26^{\text{m}}07^{\text{s}}.4 + 17^{\circ}21'05''.0$  (J2000.0). Trujillo et al. (2001) made CCD image observations in the central ( $2.5' \times 2.5'$ ) region of the cluster and provided a quantitative morphological analysis of the galaxies. The brightest galaxy (PGC 068859) is classified as a cD galaxy. The spectroscopic survey provided 12 members of the cluster with velocity dispersion  $\sigma_v = 880 \text{ km s}^{-1}$  (Miller et al. 2002).

---

\* Supported by the National Natural Science Foundation of China.

X-ray observation by ROSAT satellite reveals a clump of hot gas associated with the central cD galaxy (Ebeling 1996). Additionally, a search utilizing the NASA/IPAC Extragalactic Database (NED) indicates that the galaxy cluster ZwCl 2224.2+1651 (Zwicky et al. 1965), located at  $22^{\text{h}}26^{\text{m}}37^{\text{s}}.6 +17^{\circ}06'18''$ , is 15.7 arcmin away from the center of A2443, but it is still not known whether the cluster interacts with A2443.

Although optical spectroscopic observation is the most powerful approach for the cluster membership determination, spectroscopy of faint galaxies in a cluster remains a rather daunting task. When spectroscopic identifications are not available for a large number of cluster galaxies, photometric redshift technique can be used to find faint cluster members on the basis of their SEDs (e.g., Pelló et al. 1999a; Brunner & Lubin 2000). In this paper, we present an intermediate-band photometric study of the galaxy cluster A2443 based on the BATC system. With 14-band photometry, the Beijing-Arizona-Taiwan-Connecticut (BATC) system is suited for photometric redshift determination. Xia et al. (2002) applied Monte Carlo simulation to estimate the uncertainty in the photometric redshifts with the BATC system, and the result showed that the accuracy can reach  $\sigma_z \sim 0.02 - 0.03$  for magnitude errors from 0.05 to 0.1 mag. Such accuracy allows us to study some statistical properties in nearby rich clusters (Yuan et al. 2001, 2003; Zhou et al. 2003b; Yang et al. 2004).

This paper is organized as follows: We describe the observations and data reduction in Section 2. The membership determination of A2443 is given in Section 3. The properties of A2443: the luminosity function, color-magnitude relation, spatial distribution and star formation history are analyzed in Section 4. Our discussion is given in Section 5. Finally, we summarize our work in Section 6. Throughout this paper we adopt the  $\Lambda$ CDM cosmology model with  $H_0 = 75 \text{ km s}^{-1} \text{ Mpc}^{-1}$ ,  $\Omega_m = 0.3$  and  $\Omega_\Lambda = 0.7$ .

## 2 OBSERVATION AND DATA REDUCTION

### 2.1 Observation

The BATC multi-color sky survey is carried out with the 60/90 cm f/3 Schmidt telescope of the National Astronomical Observatories, Chinese Academy of Sciences (NAOC), located at the Xinglong station. A Ford Aerospace 2048  $\times$  2048 CCD camera of  $15 \mu\text{m}$  pixel size is mounted at the main focus of the telescope. The field of view is  $58' \times 58'$ , with a scale of  $1.7'' \text{ pixel}^{-1}$ . The BATC filter system contains 15 intermediate-band filters covering the wavelength range from 3000 to 10000  $\text{\AA}$ . These filters were especially designed to avoid bright night sky emission lines (Fan et al. 1996). The transmission curves can be seen from figure 1 of Xia et al. (2002).

**Table 1** Parameters of BATC Filters and Statistics of Observations

| No. | Filter Name | $\lambda_c^a$<br>( $\text{\AA}$ ) | FWHM<br>( $\text{\AA}$ ) | Exposure<br>(s) | $N_1^b$ | Seeing <sup>c</sup><br>(arcsec) | $N_2^d$ |
|-----|-------------|-----------------------------------|--------------------------|-----------------|---------|---------------------------------|---------|
| 1   | <i>b</i>    | 3890                              | 291                      | 15000           | 19      | 5.53                            | 3       |
| 2   | <i>c</i>    | 4210                              | 309                      | 5100            | 7       | 5.36                            | 2       |
| 3   | <i>d</i>    | 4550                              | 332                      | 17760           | 18      | 3.88                            | 3       |
| 4   | <i>e</i>    | 4920                              | 374                      | 12900           | 12      | 4.30                            | 1       |
| 5   | <i>f</i>    | 5270                              | 344                      | 12180           | 13      | 4.57                            | 3       |
| 6   | <i>g</i>    | 5795                              | 289                      | 15240           | 15      | 4.68                            | 2       |
| 7   | <i>h</i>    | 6075                              | 308                      | 4440            | 6       | 3.68                            | 3       |
| 8   | <i>i</i>    | 6660                              | 491                      | 16680           | 20      | 5.21                            | 5       |
| 9   | <i>j</i>    | 7050                              | 238                      | 20040           | 20      | 5.30                            | 3       |
| 10  | <i>k</i>    | 7490                              | 192                      | 10080           | 12      | 3.77                            | 2       |
| 11  | <i>m</i>    | 8020                              | 255                      | 12480           | 14      | 4.74                            | 3       |
| 12  | <i>n</i>    | 8480                              | 167                      | 4380            | 5       | 4.61                            | 1       |
| 13  | <i>o</i>    | 9190                              | 247                      | 17400           | 16      | 4.23                            | 1       |
| 14  | <i>p</i>    | 9745                              | 275                      | 900             | 2       | 4.49                            | 2       |

<sup>a</sup> Central wavelength of filter; <sup>b</sup> Number of observed images of each filter; <sup>c</sup> Seeing of combined images; <sup>d</sup> Number of calibration images.

Images of A2443 in the 14 bands were obtained with total exposure time more than 40 hours from September 1995 to September 1998 (see the observational statistics in Table 1). We carried out the standard data reduction procedures of bias subtraction, flat-fielding correction, and position calibration. Cosmic rays and bad pixels were removed by comparing multiple images during combination. The special photometry package, PIPELINE2, developed for detecting and measuring the flux of sources, was used with brightness above a threshold within a given aperture in the BATC images (Zhou et al. 2003a). An object is considered to be detected if its signal to noise ratio is larger than the threshold  $3.5\sigma$  in  $i$ ,  $j$  and  $k$  bands, and a radius of 4 pixels ( $6.8''$ ) is adopted as the photometric aperture. The flux calibration was performed using the Oke-Gunn primary flux standard star HD 19445, HD 84937, BD+26 2606 and BD+17 4708 (Gunn & Stryker 1983). The procedures of BATC flux calibration are described by Zhou et al. (2001). As a result, the SEDs of 5975 sources brighter than  $i = 20.0$  mag have been obtained.

## 2.2 Star-Galaxy Separation

The average seeing is  $5.2''$  (FWHM) in the  $i$  band images, which means that any smaller image cannot discriminate between a galaxy or a star. However, the SED information contained in the BATC filters can help our separation since the spectra of redshifted galaxies differ significantly from those of stars. As shown in Yuan et al. (2001), the redshifted galaxies can be well separated from stars in the color-color diagrams.

First, we use 145 confirmed galaxies to check the reliability of our star-galaxy separation in color-color diagrams. This sample includes 70 galaxies from the 2 Micron All Sky Survey Extended objects (2MASX) and Trujillo et al. (2001), and the remaining 75 galaxies are selected according to their morphologies on the BATC images. Figure 1 shows two color-color diagrams used for star-galaxy separation. The diagrams include three categories of sources: (1) all types of stars in the SED template library (Pickles 1998) (denoted by filled triangles), (2) the confirmed galaxy sample (denoted by asterisks), (3) sources detected by the photometric measurements (denoted by small dots). Four bands are used in the diagrams:  $f$  ( $5270 \text{ \AA}$ ),  $h$  ( $6075 \text{ \AA}$ ),  $o$  ( $9190 \text{ \AA}$ ) and  $p$  ( $9745 \text{ \AA}$ ). The ellipse marks the location of galaxies between  $0.05 < z < 0.15$  using Bruzual & Charlot (1993) spectral synthesis models, and the low redshift galaxy models are distributed at the top-left. Since most galaxies detected in our images are nearby ( $z < 0.2$ ), they are expected to occupy a certain region in the color-color diagram. The dashed line box defines the boundary of star-galaxy separation according to the distribution of the confirmed galaxies. Most galaxies are distributed in

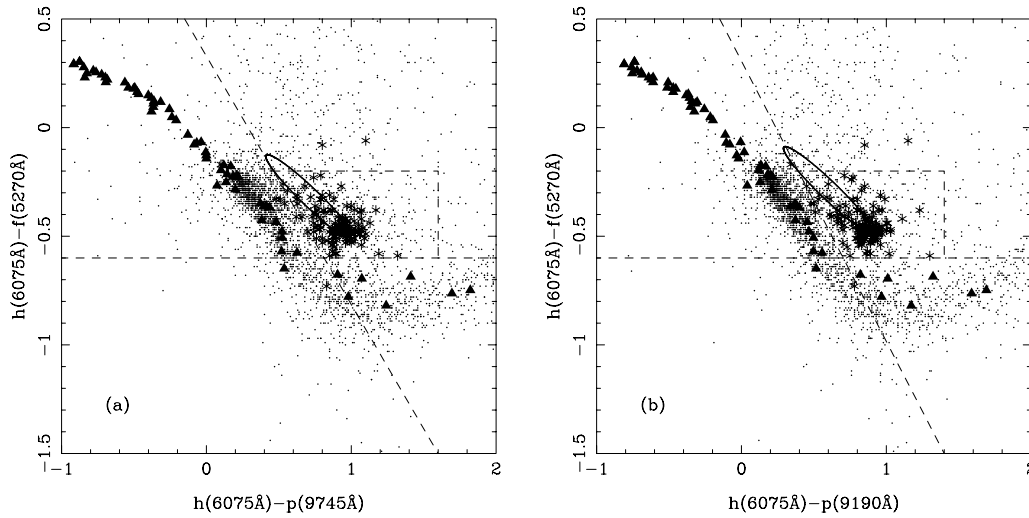


**Fig. 1** Color-color diagrams used for star-galaxy separation. Filled triangles for all types of stars in the SED template library, asterisks for the confirmed galaxies, small dots for the detected sources. The ellipse marks the location of synthesis galaxy models between  $0.05 < z < 0.15$ . The dashed line box marks the boundaries of star-galaxy separation.

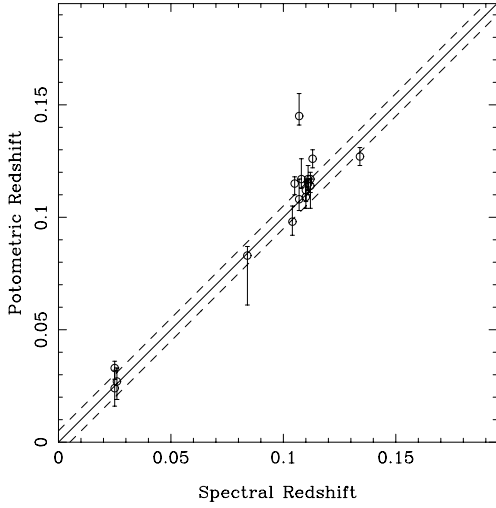


**Fig. 2** Comparison between photometric redshift  $z_{\text{phot}}$  and spectroscopic redshift  $z_{\text{spec}}$  for 17 known galaxies in the field of view. The solid line corresponds to  $z_{\text{phot}} = z_{\text{spec}}$ , and the dashed lines indicate deviation of 0.005.

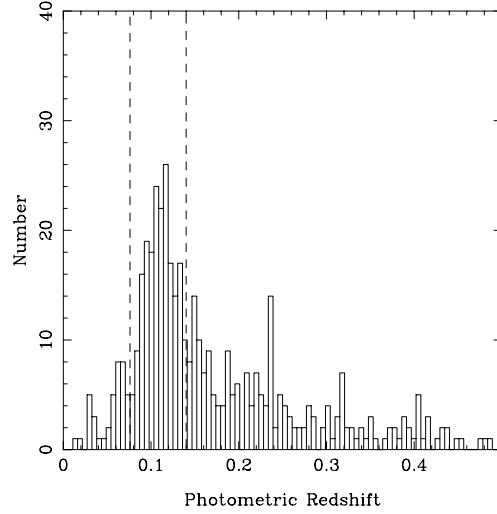


**Fig. 3** Distribution of photometric redshift for the galaxies within  $r < 2$  Mpc region. The dashed lines are plotted as the photometric redshift range of cluster member candidates.

a tight concentration in the diagram, suggesting that Figure 1 can give a satisfactory separation of nearby galaxies. As a result, 863 galaxies including the confirmed sample are separated from Figure 1(a), and 234 galaxies beyond detection in the  $p$  band are separated from Figure 1(b). Thus, we have obtained a sample of 1097 galaxies in the field of  $\sim 1\text{deg}^2$ , to which we shall apply our photometric redshift technique.

### 3 PHOTOMETRIC REDSHIFTS AND CLUSTER MEMBERSHIP

Photometric redshift technique has been used to search for high- $z$  objects (Pelló et al. 1999a, b; Bolzonella et al. 2000) and to determine galaxy cluster membership (Brunner & Lubin 2000). Photometric redshift is derived with the standard SED-fitting code HYPERZ (Bolzonella et al. 2000). The algorithm minimizes the standard  $\chi^2$  between the observed SEDs and the template SEDs of galaxy spectra,

$$\chi^2 = \sum_{i=1}^{N_f} \left[ \frac{F_i^{\text{obs}} - bF_i^{\text{temp}}}{\sigma_i} \right]^2, \quad (1)$$

where  $N_f$  is the number of filters;  $F_i^{\text{obs}}$ ,  $F_i^{\text{temp}}$  and  $\sigma_i$  are the observed SED, template SED and photometric error in the  $i$ th filter, respectively;  $b$  is the normalization factor. Previous work has evaluated the accuracy of photometric redshift with BATC multi-band data (Yuan et al. 2001, 2003; Zhou et al. 2003b; Yang et al. 2004). A comparison of photometric redshift  $z_{\text{phot}}$  versus spectroscopic redshift  $z_{\text{spec}}$  of 17 bright galaxies in the A2443 field is given in Figure 2, showing a deviation of 0.01. The dash lines indicate deviation of 0.005.

Figure 3 shows the photometric redshift histogram of galaxies in the central region ( $r < 2$  Mpc) of A2443. Galaxies with photometric redshifts between  $\bar{z} \pm 3\sigma_z$  ( $0.08 < z_{\text{phot}} < 0.14$ ) are selected as member candidates of A2443. As a result, 301 member candidates including 12 known members are obtained.<sup>1</sup>

<sup>1</sup> The SED catalog is published as online data ([http://www.chjaa.org/2007\\_7.1.htm](http://www.chjaa.org/2007_7.1.htm))

## 4 RESULTS

### 4.1 Luminosity Function and Color-Magnitude Relation

The luminosity function (LF) of cluster galaxies describes the luminosity distribution of the cluster population. It is a fundamental constraint on the mass assembly history of cluster galaxies as it is related to the mass function of galaxies (Goto et al. 2005). Many previous results (e.g., Thompson & Gregory 1980; Biviano et al. 1996) showed that the LF of cluster galaxies can be described by Schechter function (Schechter 1976):

$$\phi(L)dL = \phi^*(L/L^*)^\alpha \exp(-L/L^*)d(L/L^*), \quad (2)$$

where  $\phi^*$ ,  $L^*$ ,  $\alpha$  are the normalization parameter, characteristic luminosity and faint slope parameter, respectively. For the following analysis, we transform the BATC magnitudes of the member galaxies into the conventional Kron-Cousins  $V$ ,  $R$  and  $I$  magnitudes via the equations given in Zhou et al. (2003a). Figure 4 shows the LF of galaxies in  $r < 2$  Mpc region of A2443 (we apply  $k$ -corrections explored by Fukugita et al. 1995). The solid curve shows the best-fit Schechter function with  $M^* = -20.8$  and  $\alpha = -0.83$ .

The sample of cluster members allows us to establish the color-magnitude (CM) relation of A2443 shown in Figure 5. A least-square fit of the linear relation between  $e(4920 \text{ \AA}) - k(7490 \text{ \AA})$  and  $i(6660 \text{ \AA})$  for the galaxies with magnitude  $i < 18.5$  and  $e - k > 1.0$  within  $r < 2$  Mpc region gives  $(e - k) = -0.026(\pm 0.014)i + 1.61(\pm 0.10)$ . Note we have corrected the Galactic extinction using the extinction curve of Cardelli et al. (1989) and we adopt the value of  $E(B - V) = 0.062$  given by Schlegel et al. (1998). To compare with previous results, a linear fit of  $(V - I) = -0.024(\pm 0.019)V + 1.77(\pm 0.035)$  is obtained with the transformed magnitudes. This slope is consistent with that of Fornax early-type galaxies (Karick et al. 2003).

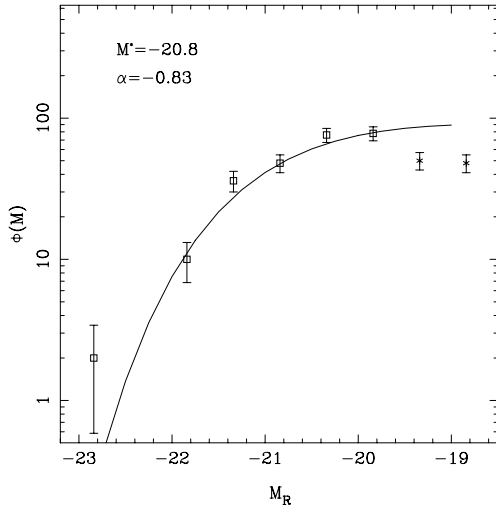


**Fig. 4** LF of A2443. The solid curve indicates the best-fit Schechter function whose parameters are shown in the top-left of plot. The error bars represent the associated Poissonian errors. Two points of the faint end are not included in the fitting.

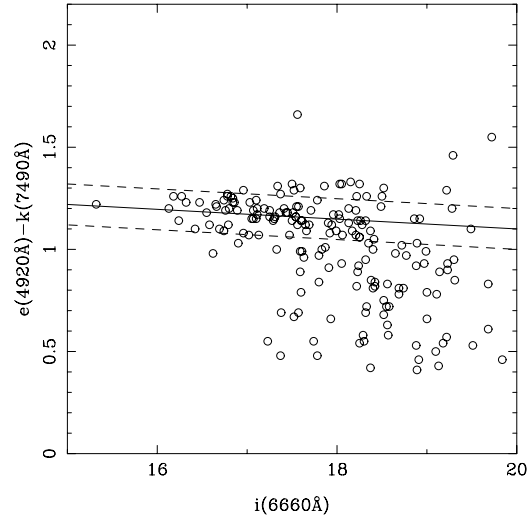


**Fig. 5** Color-magnitude diagram for A2443 galaxies. The solid line shows the linear fit for galaxies brighter than  $i = 18.5$  and  $e - k > 1.0$  within  $r < 2$  Mpc region, and the dash lines correspond to the  $1\sigma$  dispersion.

### 4.2 Spatial Distribution

The global morphology of A2443 is shown in Figure 6, superposed with a contour map, with contour levels 0.12, 0.24, 0.36, 0.48, 0.6 and 0.72  $\text{arcmin}^{-2}$ . It shows an elongated distribution along the NW-SE direction, with few galaxies located in the northern east and southern west. To investigate the distribution

of different type galaxies, we have defined blue galaxies to be those with color indexes ( $e - k$ ) bluer than the ridge line of the fitted CM relation by  $2\sigma$ . In Figure 6, the blue and red galaxies are marked with open and filled circles, the cD galaxy and the density peak are marked with a filled triangle and an open square. Two X-ray emission peaks observed by ROSAT are shown. The dash line is plotted to separate out the SE subgroup. It is obvious that the red galaxies are clustered in the core region, whereas the blue galaxies are scattered throughout: this is also shown by their surface density profiles in Figure 7. This result apparently suggests that blue galaxies are distributed in the outer region of the cluster.

In order to give a quantitative measurement of A2443's elongated morphology, we calculate the cluster ellipticity with the method introduced by Carter & Metcalfe (1980). The position (RA, Dec.) of each galaxy is transformed into Cartesian coordinates ( $x, y$ ), and we compute the moment as

$$I_{11} = \frac{1}{N} \sum_{i=1}^N x_i^2 - \bar{x}^2, \quad (3)$$

$$I_{22} = \frac{1}{N} \sum_{i=1}^N y_i^2 - \bar{y}^2, \quad (4)$$

$$I_{12} = I_{21} = \frac{1}{N} \sum_{i=1}^N x_i y_i - \bar{x} \bar{y}. \quad (5)$$

We solve the quadratic equation  $\det(I_{ij} - \lambda^2 M_2) = 0$  ( $M_2$  being the  $2 \times 2$  unit matrix), and obtain the eigenvalues  $\lambda_1, \lambda_2$  (let  $\lambda_1 > \lambda_2$ ). The position angle of the major axis with respect to the north is derived from

$$\theta = \cot^{-1} \left( \frac{\lambda_1^2 - I_{22}}{I_{11}} \right) + \frac{\pi}{2}, \quad (6)$$

and the ellipticity is calculated as

$$\epsilon = 1 - \frac{\lambda_2}{\lambda_1}. \quad (7)$$

We apply these equations on the sample of galaxies within  $r < 2$  Mpc of A2443 and obtain the ellipticity  $\epsilon = 0.30$  and position angle  $\theta = 39^\circ$ .

Another related quantity characterizing the degree of asymmetry, the shift of the center-of-mass position ( $sc$ ), is defined as the distance between the center-of-mass ( $x_0, y_0$ ) and the density-peak ( $x_p, y_p$ ) by Evrard et al. (1993) and Mohr et al. (1993). Following their definition, we calculate the centroid-shift  $sc_o = \sqrt{(x_0 - x_p)^2 + (y_0 - y_p)^2}$ , and found  $sc_o = 0.13$  Mpc. To quantify its significance we made a Monte Carlo simulation with mock clusters with a King profile. We took  $r_c = 0.32$  Mpc (Dressler 1978) and made 1000 simulations to derive the mean value  $\langle sc \rangle_{\text{sim}}$  and the standard variance  $\sigma_{\text{sim}}$ . Then we calculate the quantity

$$\sigma = \frac{sc_o - \langle sc \rangle_{\text{sim}}}{\sigma_{\text{sim}}}. \quad (8)$$

The result shows a significance of  $\sigma = 5.4$ . We also use  $r_c = 0.43$  Mpc derived from the BATC data. The significance then changes to  $\sigma = 4.6$ .

### 4.3 STAR FORMATION HISTORY

We use an evolutionary synthesis model, PEGASE (Fioc & Rocca-Volmerange 1997) to investigate the star formation history of A2443. This method requires stellar initial mass function (IMF), star formation rate (SFR) and metallicity as input parameters. Each galaxy template is defined by the form of SFR and metallicity  $Z$ . In the model the synthetic stellar spectral library is taken from Kurucz (1992). We choose a Salpeter (1955) initial mass function and an SFR in the form of  $e^{-t/\tau}$ , with time scale  $\tau$  in the range of 0–30 Gyr. To avoid degeneracy between age and metallicity in the model, we adopt an age of nearby cluster galaxies of 11.4 Gyr as derived by Thomas et al. (2005) and an initial metallicity of  $Z = 0.0001$ . We determine the time scale  $\tau$  for each galaxy by comparison between the templates and observed SEDs.

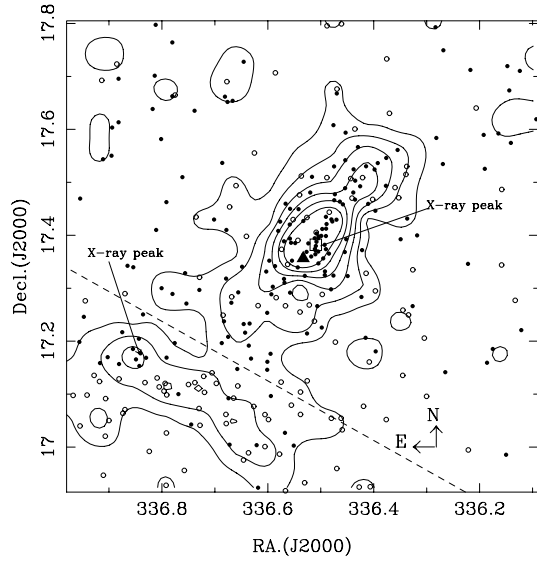


**Fig. 6** Spatial distribution of A2443 member candidates. Blue and red galaxies are marked with open and filled circles, respectively. The cD galaxy PGC 068859 is marked with a filled triangle and the density peak, with an open square. Two X-ray peaks observed by ROSAT are also shown. The dash line is plotted to separate out the SE subgroup. The corresponding contour map is superposed on the galaxy distribution with contour levels 0.12, 0.24, 0.36, 0.48, 0.6 and 0.72  $\text{arcmin}^{-2}$ .

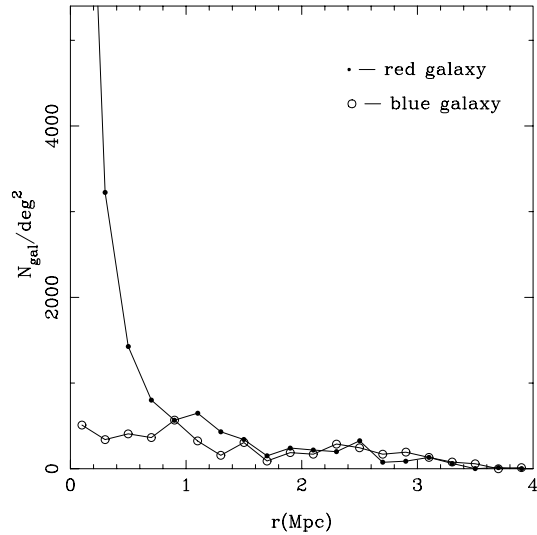


**Fig. 7** Surface density profiles for the red (filled circles) and blue (open circles) galaxies.

Figure 8 shows the time scales of star formation with error less than 10 Gyr for the galaxies within  $r < 2$  Mpc region as a function of  $M_R$ . The red and blue galaxies are denoted with filled and open circles, respectively. The dash line shows the typical value ( $\tau = 1.2$  Gyr) for the red galaxies. It shows that the faint galaxies ( $M_R > -21$ ) tend to have longer time scales of star formation than the bright ones, indicating that faint galaxies differ from bright ones in their evolutionary history. Tajiri & Kamaya (2001) suggested that cluster galaxies brighter than  $M_R = -20.7$  have suppressed SFRs, and this is consistent with our result.

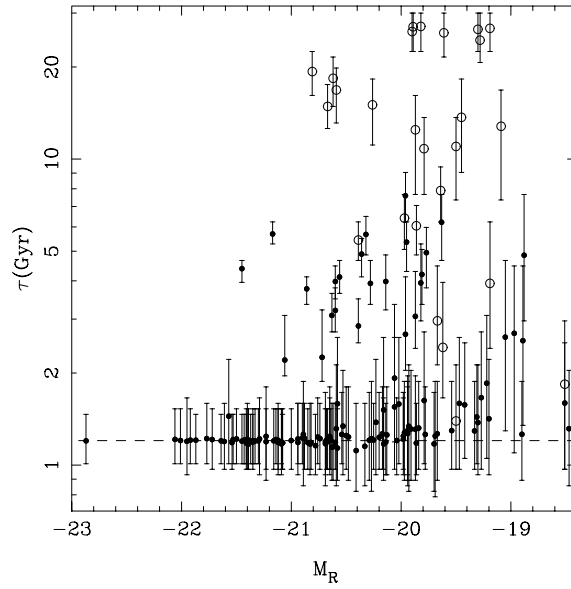


**Fig. 8** Time scale of star formation with error less than 10 Gyr for the galaxies within  $r < 2$  Mpc as a function of absolute magnitude  $M_R$ . Blue and red galaxies are marked with open and filled circles, respectively. The dash line plots  $\tau = 1.2$  Gyr.

## 5 DISCUSSION

We performed galaxy-star separation using color-color diagrams. Sources in the box of Figure 1 are picked out as nearby galaxies. Higher redshift galaxies possibly are missed, but they are not taken into account in this study. A certain fraction of nearby faint galaxies could lie outside of the box of Figure 1 due to errors. They would not have been determined as candidates of A2443 even if they were members. This is one possible reason that the faint end of our LF is lower than that of Pracy et al. (2005). On the other hand, a few stars with red colors may lie inside the box we set, so our galaxies could include some red stars, to which we apply HYPERZ as galaxies. Assume their “photometric redshifts” are randomly distributed between 0 and 0.5, one-eighth of the false galaxies would have been considered as candidates of A2443. These stars should be distributed randomly on the sky, and so will not affect the cluster morphology.

An elongated galaxy distribution is shown in the field of A2443. Most of the galaxies are located in one main cluster and a connecting subgroup. The ROSAT observation shows that a weak clump of X-ray emission is located in the SE subgroup. It is the galaxy cluster ZwCl 2224.2+1651 and the X-ray emission peak is located at  $22^{\text{h}}27^{\text{m}}14^{\text{s}}.5 + 17^{\circ}06'02.2''$ . The projected distance between two X-ray peaks in Figure 6 is 2.5 Mpc, and their position angle is consistent with the cluster elongated morphology. This may indicate that ZwCl 2224.2+1651 is at the stage of falling into A2443.

It should be noted that the fraction of blue galaxies in ZwCl 2224.2+1651 is much higher than in the main cluster of A2443. This may suggest that there are recent star formation activities. One hypothesis is that cluster-cluster interaction triggers the star formation when ZwCl 2224.2+1651 moves close to A2443. Similar results have been shown in many merging nearby rich clusters. Metevier et al. (2000) found the fractions of blue galaxies in on-going merging clusters are higher, and suggested that star formation is occurring due to the cluster-cluster merging. Caldwell et al. (1993) showed that strong Balmer-line absorption galaxies are distributed between the main Coma cluster and a merging subcluster. Recent study showed that in A3921 most of the emission line galaxies and blue galaxies lie in the region of the smaller subcluster, and in the region between two subclusters (Ferrari et al. 2005). Possible physical mechanisms to explain the star formation activity within the merging clusters are tidal gravitational field (e.g. Bekki 1999) and the increased external pressure (Dressler & Gunn 1983; Evrard 1991).

## 6 SUMMARY

We present a photometric study of A2443 with the BATC 14-intermediate band system. The images of BATC A2443 field were accumulated with a total exposure time of more than 40 hours. The SEDs of 5975 detected sources brighter than 20.0 mag in  $i$  band were obtained above a  $3.5\sigma$  detection threshold. Color-color diagrams were used for star-galaxy separation. From this, we obtained 1097 galaxies in the field of  $\sim 1 \text{ deg}^2$ . By using a photometric redshift technique, we were able to obtain a sample of 289 new member candidates.

Based on the enlarged sample, we fit the LF of A2443 with a Schechter function, and established the color magnitude relation. A linear fit of the CM relation shows a similar slope to the Fornax cluster. Morphologically we find an elongated structure of galaxy distribution. Red galaxies are strongly clustered, and blue galaxies are distributed homogeneously. We measured the shape of the cluster, giving the ellipticity and the shift of the center-of-mass position. Our results also indicate that galaxy cluster ZwCl 2224.2+1651 may be falling into A2443, and cluster-cluster interaction could trigger star formation in ZwCl 2224.2+1651. Stellar population synthesis was applied to investigate the cluster galaxies star formation history. With an exponential star formation rate, we found that the fainter galaxies ( $M_R > -21$ ) tend to have longer time scales of star formation than the brighter ones.

**Acknowledgements** We are grateful to David Burstein for his valuable suggestions. We thank Jiuli Li, Tianmeng Zhang, Lifang Xia and Zhiyu Duan for helpful and inspiring discussions. We would like to express our gratitude to all the assistants who contributed with their hard work to the observations. This work is supported by the National Natural Science Foundation of China (NSFC, Nos. 10473012, 10273007 and 10633020) and the National Key Basic Research Science Foundation (NKBRSF, TG199075402). This research has made use of the NED, which is operated by the Jet Propulsion Laboratory, California Institute of Technology, under contract with the National Aeronautics and Space Administration.

## References

- Abell G. O., 1958, ApJS, 3, 211  
 Bahcall N. A., 1988, ARA&A, 26, 631  
 Baier F. W., 1977, Astronomische Nachrichten, 298, 151  
 Bekki K., 1999, ApJ, 510, L15  
 Bird C. M., 1994, AJ, 107, 1637  
 Biviano A., Durret F., Gerbal D. et al., 1996, Astrophysical Letters Communications, 33, 223  
 Bolzonella M., Miralles J. M., Pelló R., 2000, A&A, 363, 476  
 Brunner R. J., Lubin L. M., 2000, AJ, 120, 2851  
 Bruzual A., G., Charlot S., 1993, ApJ, 405, 538  
 Caldwell N., Rose J. A., Sharples R. M., Ellis R. S., Bower R. G., 1993, AJ, 106, 473  
 Cardelli J. A., Clayton G. C., Mathis J. S., 1989, ApJ, 345, 245  
 Carter D., Metcalfe N., 1980, MNRAS, 191, 325  
 Colberg J. M., White S. D. M., Yoshida N. et al., 2000, MNRAS, 319, 209  
 Colless M., Dunn A. M., 1996, ApJ, 458, 435  
 Cortese L., Gavazzi G., Boselli A., Iglesias Paramo J., Carrasco L., 2004, A&A, 425, 429  
 Dressler A., 1978, ApJ, 226, 55  
 Dressler A., Gunn J. E., 1983, ApJ, 270, 7  
 Dressler A., Shectman S. A., 1988, AJ, 95, 284  
 Ebeling H., Voges W., Bohringer H., Edge A. C., Huchra J. P., Briel U. G., 1996, MNRAS, 281, 799  
 Escalera E., Biviano A., Girardi M. et al., 1994, ApJ, 423, 539  
 Evrard A. E., 1991, MNRAS, 248, 8P  
 Evrard A. E., Mohr J. J., Fabricant D. G., Geller M. J., 1993, ApJ, 419, L9  
 Fan X., Burstein D., Chen J. S. et al., 1996, AJ, 112, 628  
 Ferrari C., Benoist C., Maurogordato S., Cappi A., Slezak E., 2005, A&A, 430, 19  
 Floc M., Rocca-Volmerange B., 1997, A&A, 326, 950  
 Fukugita M., Shimasaku K., Ichikawa T., 1995, PASP, 107, 945  
 Goto T., Postman M., Cross N. J. G. et al., 2005, ApJ, 621, 188

- Gunn J. E., Stryker L. L., 1983, *ApJS*, 52, 121  
Karick A. M., Drinkwater M. J., Gregg M. D., 2003, *MNRAS*, 344, 188  
Kauffmann G., Colberg J. M., Diaferio A., White S. D. M., 1999, *MNRAS*, 303, 188  
Kurucz R. L., 1992, *IAU Symp. 149: The Stellar Populations of Galaxies*, 149, 225  
McHardy I. M., 1974, *MNRAS*, 169, 527  
Metevier A. J., Romer A. K., Ulmer M. P., 2000, *AJ*, 119, 1090  
Miller C. J., Krughoff K. S., Batuski D. J., Hill J. M., 2002, *AJ*, 124, 1918  
Mohr J. J., Fabricant D. G., Geller M. J., 1993, *ApJ*, 413, 492  
Nikogosyan E., Durret F., Gerbal D., Magnard F., 1999, *A&A*, 349, 97  
Pearce F. R., Thomas P. A., Couchman H. M. P., Edge A. C., 2000, *MNRAS*, 317, 1029  
Pelló R., Kneib J. P., Le Borgne J. F. et al., 1999a, *A&A*, 346, 359  
Pelló R., Kneib J. P., Bolzonella M., Miralles J. M., 1999b, *ASP Conf. Ser.* 191, 241  
Pickles A. J., 1998, *PASP*, 110, 863  
Postman M., Huchra J. P., Geller M. J., 1992, *ApJ*, 384, 404  
Pracy M. B., Driver S. P., De Propris R. et al., 2005, *MNRAS*, 364, 1147  
Salpeter E. E., 1955, *ApJ*, 121, 161  
Schechter P., 1976, *ApJ*, 203, 297  
Schlegel D. J., Finkbeiner D. P., Davis M., 1998, *ApJ*, 500, 525  
Struble M. F., Rood H. J., 1999, *ApJS*, 125, 35  
Tajiri Y. Y., Kamaya H., 2001, *ApJ*, 562, L125  
Thomas D., Maraston C., Bender R., de Oliveira C. M., 2005, *ApJ*, 621, 673  
Thompson L. A., Gregory S. A., 1980, *ApJ*, 242, 1  
Trujillo I., Aguerri J. A. L., Gutiérrez C. M., Cepa J., 2001, *AJ*, 122, 38  
West M. J., Villumsen J. V., Dekel A., 1991, *ApJ*, 369, 287  
West M. J., Jones C., Forman W., 1995, *ApJ*, 451, L5  
Xia L., Zhou X., Ma J. et al., 2002, *PASP*, 114, 1349  
Yang Y., Zhou X., Yuan Q. et al., 2004, *ApJ*, 600, 141  
Yuan Q., Zhou X., Chen J. et al., 2001, *AJ*, 122, 1718  
Yuan Q., Zhou X., Jiang Z., 2003, *ApJS*, 149, 53  
Zhou X., Jiang Z., Xue S. et al., 2001, *Chin. J. Astron. Astrophys. (ChJAA)*, 1, 372  
Zhou X., Jiang Z., Ma J. et al., 2003a, *A&A*, 397, 361  
Zhou X., Arimoto N., Tanaka I., Jiang Z., Chen J., 2003b, *PASJ*, 55, 891  
Zeldovich I. B., Einasto J., Shandarin S. F., 1982, *Nature*, 300, 407  
Zwicky F., Karpowicz M., Kowal C. T., 1965, *Catalogue of Clusters of Galaxies* 5